Hindawi
Journal of Advanced Transportation
Volume 2023, Article ID 5583081, 18 pages
https://doi.org/10.1155/2023/5583081

Research Article

Exploring Heterogeneity in Car-Following Behaviors Based on Driver Visual Characteristics: Modeling and Calibration

Congcong Bai [1,2] Jun Jing,[3] Bokun Liu,[4] Wenbin Yao [1] Chengcheng Yang,[1] Adjé Jérémie Alagbé,[1] and Sheng Jin [1,2,5]

[1] *Institute of Intelligent Transportation Systems, College of Civil Engineering and Architecture, Zhejiang University, Hangzhou 310058, China*
[2] *Zhejiang Provincial Engineering Research Center for Intelligent Transportation, Hangzhou 310058, China*
[3] *Polytechnic Institute & Institute of Intelligent Transportation Systems, Zhejiang University, Hangzhou 310058, China*
[4] *China Power Construction Group East China Survey Design Institute, Zhejiang 311122, China*
[5] *Zhejiang University Zhongyuan Institute, Zhengzhou 450000, China*

Correspondence should be addressed to Sheng Jin; jinsheng@zju.edu.cn

Received 8 September 2023; Revised 24 October 2023; Accepted 1 November 2023; Published 14 November 2023

Academic Editor: Jose E. Naranjo

To investigate the heterogeneity of car-following behaviors across different vehicle combinations from the perspective of driver visual characteristics, the NGSIM dataset from I-80 and US-101 highways was selected and distinct car-following segments were extracted for analysis. Firstly, all the effective vehicle trajectories were extracted and categorized into different vehicle types based on their widths, resulting in four combination types of car-following segments. Visual angle and its change rate were introduced as variables representing driver visual characteristics. Additionally, one-way analysis of variance (ANOVA) was used to compare these variables with traditional ones. The driver's visual characteristic variables were then incorporated to improve the full velocity difference (FVD) model. Genetic algorithms were employed to calibrate the model under different car-following types, revealing pronounced behavioral variations. After implementing the enhanced drivers' visual angle (DVA) model, substantial reductions in calibration and validation errors were observed, with calibration errors decreasing by 51.93% and 42.22% and validation errors decreasing by 56.61% and 45.26%. This indicates the DVA model's remarkable adaptability and stability. Lastly, through a sensitivity analysis of errors, the DVA model demonstrated greater robustness toward the improved error evaluation function. By integrating drivers' visual characteristics, this study provides in-depth insights into heterogeneous car-following behaviors, enhancing our understanding of driver behaviors and micro-traffic simulation systems.

1. Introduction

Car-following models have long been a focal point in the field of traffic flow theory. By modeling car-following behaviors, it becomes possible to quantify the longitudinal interactions between following vehicles (FVs, the vehicles located behind in the process of car-following, will receive the stimulus of the front car and produce a response) and leading vehicles (LVs, the leading vehicles in the process of car-following, which can bring certain stimulation to the FVs), thereby deciphering the operational characteristics of traffic flow and revealing the underlying mechanisms of micro-level driving behaviors. Since the inception of the car-following concept by Pipes [1], more than 70 years of development have transpired. Numerous car-following models have been proposed and gradually refined, with scholars like Dian-hei and Sheng [2] systematically categorizing and delineating these models from both traffic engineering and statistical physics perspectives. With the advent of big data and the rise of technologies such as machine learning and deep learning, various data-driven car-following model theories and trajectory prediction methods [3–6] have emerged. However, amidst the rapid theoretical progress of these models, their physical significance and interpretability have gradually waned, and attributes like driver characteristics and vehicle heterogeneity have been overlooked. Nevertheless, human-driven vehicles remain the primary actors in road traffic flow. Hence, drivers continue to be the most crucial element within road traffic components. Yao et al. [7] assessed patterns of individual emergence during the pandemic; Qu et al. [8] explored how ridership contributes to the planning and operation of urban and rural bus systems, showing that individual behavior rules can affect macro-traffic conditions. Tang et al. [9] introduced drivers' bounded rationality into the speed guidance model and demonstrated through simulation results that drivers' bounded rationality significantly impacts vehicle fuel consumption and emissions. Jin et al. [10] studied drivers' behavior of using mobile phones at intersections, and the results show that using mobile phones has a significant negative impact on driving behavior. Furthermore, Liao et al. [11] improved the traditional car-following model by taking into account drivers' driving habits, enhancing the model's safety and comfort. To better describe the impact of the driver's stochastic characteristics on car-following behaviors, Luo et al. [12] proposed a stochastic full velocity difference model (SFVDM) considering the stochastic variation of the desired velocity. Accurately comprehending the driving mechanisms of drivers during the driving process and establishing behavior models that are closer to real-world driving scenarios from a driver's perspective hold significant importance for a deeper understanding of driving behavior mechanisms and micro-traffic simulation systems [13].

Conventional car-following models frequently assume homogeneity among both drivers and vehicles. However, in real-world scenarios, the presence of driver individuality, vehicle disparities, and even environmental distinctions such as weather and road conditions introduce heterogeneity into car-following behaviors. This heterogeneity is closely associated at a macroscopic level with phenomena including the reduction of road capacity, traffic congestion, traffic oscillations, and the emergence of stop-and-go waves [14, 15]. Ossen and Hoogendoorn [16] designated this form of heterogeneity as the divergences in car-following behavior exhibited between diverse drivers or distinct vehicle combinations operating within the same environmental context (i.e., identical road segments, comparable traffic conditions, and analogous weather conditions).

At the driver level, An et al. [17] introduced a delay parameter in reaction time to capture variations in responses among drivers with different levels of experience. They formulated the extended full velocity difference (FVD) model that takes driver heterogeneity into account. Subsequently, Cheng et al. [18] investigated the differences in car-following characteristics among drivers with varying cultural backgrounds through virtual driving experiments. Pan and Guan [19] employed quantile regression to model driver heterogeneity at different quantiles. Makridis et al. [20] proposed a novel framework based on identifying driver characteristics through acceleration behavior, demonstrating driver heterogeneity in microsimulation scenarios.

At the vehicle level, Peeta et al. [21] pioneered categorizing different vehicle types into distinct car-following groups, examining differences in car-following behavior between heavy vehicles and regular automobiles. Liu et al. [22] extended the intelligent driver model (IDM) by considering various vehicle combinations (C-C, C-T, T-C, and T-T, where C represents cars and T denotes trucks). They coupled the extended model with NGSIM dataset calibration to derive corresponding fundamental traffic diagrams. Raju et al. [23], utilizing data collected from two road sections in India, introduced "lateral separation" to combinations such as C-C, C-T, T-C, and T-T and recalibrated the Wiedemann model in Vissim software.

Existing studies predominantly focus on car-following behaviors between vehicles of different functional categories, considering combinations such as cars with trucks, buses, or heavy vehicles. Nevertheless, due to the limited representation of trucks and buses in actual collected data, the sample size often fails to adequately support their conclusions. Moreover, current research predominantly centers on heterogeneity in vehicle performance and driving behaviors among different functional vehicle types. However, there is limited investigation into the heterogeneity within the same functional category of vehicles. Furthermore, considering that the primary source of stimuli for drivers is visual input, the existing research that considers vehicle types still relies on traditional car-following variables, neglecting the investigation of the visual stimuli brought about by different vehicle types on drivers.

To address these issues, this study aims to characterize the influence of heterogeneous vehicle types on car-following behaviors within the same functional category of vehicles from the perspective of drivers' visual characteristics. The study utilizes the NGSIM dataset to extract all passenger cars, categorizes them into vehicle types, and obtains four types of car-following segments. To investigate vehicle-type heterogeneity in car-following, visual characteristics are introduced as variables and subjected to numerical simulation. Single-factor analysis of variance is employed to compare the differences in car-following behavior performance between traditional car-following variables and visual characteristics. Finally, a drivers' visual angle (DVA) model incorporating visual characteristics is established, and its effectiveness is evaluated through comprehensive and type-specific calibration, validation, and error sensitivity analysis.

The contributions of this study can be summarized as follows. First, this study introduces the drivers' visual characteristic variables into the context of heterogeneous vehicle-type car-following models. Based on trajectory data, the visual angle and its rate of change are constructed to study vehicle-type heterogeneity from the perspective of drivers' visual characteristics, showcasing the effectiveness of visual characteristic variables in addressing heterogeneity in car-following scenarios. Second, an improved model is proposed based on visual characteristic variables. Through comprehensive calibration and validation, as well as validation for four different combination types, the method is proven to significantly enhance model fitting performance. Additionally, the error sensitivity analysis demonstrates the model's robustness across various road conditions, vehicle combinations, and different error evaluation criteria. Finally, the statistical analysis of visual characteristic variables and model comparison substantiate that modeling from the perspective of drivers' visual characteristics is of vital significance in enhancing model fitting performance and resolving the issue of heterogeneous car-following combination types. This study introduces novel avenues for investigating car-following behavioral heterogeneity.

The remainder of this paper is organized as follows. In Section 2, the preprocessing of trajectory data and the classification criteria of four heterogeneous car-following combination types are introduced, and the visual characteristic parameters are extracted for numerical simulation. Statistical difference analysis of heterogeneous car-following behaviors is introduced in Section 3. Section 4 elaborates the results of model calibration and verification and discusses the results. The final section concludes the study.

2. Data Description

2.1. Data Source and Trajectory Reconstruction. To investigate the impact of vehicle type heterogeneity on driver behavior, this study utilizes the publicly available Next Generation Simulation (NGSIM) dataset [24] provided by the United States Federal Highway Administration. Trajectory data from two roadways, I-80 and US-101, are selected for analysis. The dataset captures vehicle trajectories at a frequency of 10 Hz, encompassing dynamic vehicle motion information such as acceleration, velocity, and headway, as well as static vehicle attributes like width and length. These attributes are crucial for vehicle type analysis. To mitigate the influence of high-occupancy vehicle (HOV) lanes and entrance/exit ramps, analysis is confined to vehicles on lanes 2 to 5 of the selected roadways. The road configuration is illustrated in Figure 1.

The raw trajectory data are acquired through video processing software. However, inherent anomalies and random noise in the data result in significant deviations between obtained trajectories and actual trajectories. Thus, prior to utilization, corrective actions are necessary to rectify outliers and smooth noise. In this study, the abnormal data points were corrected by threshold cleaning and spline interpolation, and the noise was smoothed by symmetric exponential moving average (sEMA) [25]. Maczak et al. [26] conducted a comparative assessment of sEMA, locally weighted regression, Butterworth filters, Kalman filters, and multiple spline methods based on identical evaluation criteria. Ultimately, sEMA was determined to markedly minimize acceleration standard deviation and outlier counts. This method has since been widely adopted in subsequent analyses of NGSIM vehicle trajectory data [27, 28]. The smoothing process is outlined in equations (1) and (2).

$$X(t_i) = \frac{1}{Z}\sum_{k=i-D}^{i+D} X(t_k)\exp\left(\frac{-|i-k|}{\Delta}\right), \tag{1}$$

$$\begin{cases} Z = \displaystyle\sum_{k=i-D}^{i+D} \exp\left(\frac{-|i-k|}{\Delta}\right), \\ \Delta = \dfrac{1}{\mathrm{d}t}T_D, \\ D = \max\{3\Delta, i-1, m-i\}. \end{cases} \tag{2}$$

In equation (1), $X(t_k)$ represents the fitted driving parameters of the vehicle at time t_k, which includes position and driving speed. i denotes the sample point in the trajectory, dt is the sampling interval of 0.1 seconds, and m is the total length of the trajectory. In equation (2), D is the window width for boundary smoothing, and Δ is the window width for intermediate data smoothing. Thiemann et al. [25] conducted a comparative analysis of various window widths for displacement, velocity, and acceleration. Ultimately, they selected a displacement smoothing window T_x of 0.5 seconds, a velocity smoothing window T_v of 1.0 seconds, and an acceleration smoothing window T_a of 5.0 seconds.

The process involved selecting a random sample of vehicles from the I-80 and US-101 roadways. The smoothing of vehicle speeds and accelerations is schematically depicted in Figure 2. Subsequently, the reconstructed trajectories from the I-80 and US-101 datasets were analyzed. Prior to reconstruction, approximately 12.4% of the acceleration values exceeded 10 ft/s^2 (approximately 3.048 m/s^2). However, following the reconstruction process, the accelerations stabilized within the range of ±3 m/s^2. Moreover, the proportion of accelerations with magnitudes exceeding ±15 m/s^3 (referred to as jerk) decreased from 45.7% to 0%. This reduction underscores that the reconstructed trajectories align more closely with authentic driving scenarios.

2.2. Car-Following Segment Extraction and Classification. Following the trajectory data reconstruction, car-following segments were further extracted with constraints on car-following gap, duration, and following vehicle (FV) speed, based on the studies by Liu et al. [22] and Higgs and Abbas [29]. The criteria for defining car-following behavior in this study are as follows.

① The preceding vehicle's ID remains unchanged, ensuring that the vehicle consistently follows the LVs. ② The average speed of the FVs is ≥ 5 m/s to avoid uncertainties in car-following behavior during congested conditions. ③ The car-following gap is ≤ 120 m to ensure that the FVs operate under non-free-flow conditions. ④ The car-following duration is ≥ 30 s to ensure the stability of the car-following state. ⑤ The relative lateral displacement between the LVs and FVs is ≤ 1.5 m, ensuring that they remain in the same lane. The car-following samples extracted based on these criteria are summarized in Table 1.

Segmentation of different car-following types requires vehicle classification. Based on the distribution characteristics of vehicle width on I-80 and US-101 roads, a critical vehicle width of 1.95 meters (corresponding to the 40th percentile for I-80 and the 50th percentile for US-101) was selected to differentiate between small and large vehicle types. According to the vehicle types of the lead and following cars within car-following segments, these segments were categorized into four types: Small-Small (S-S), Small-Large (S-L), Large-Small (L-S), and Large-Large (L-L) car-following types. The statistical results for each type of car-following segment are presented in Table 2.

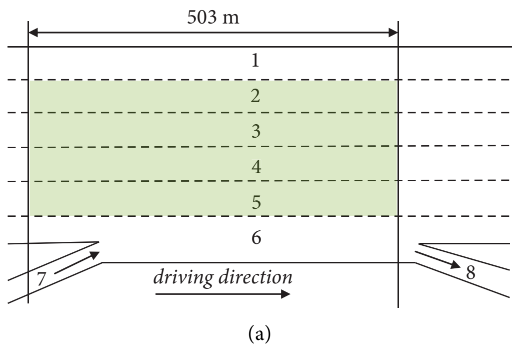

FIGURE 1: Diagram of NGSIM roads. (a) I-80. (b) US-101.

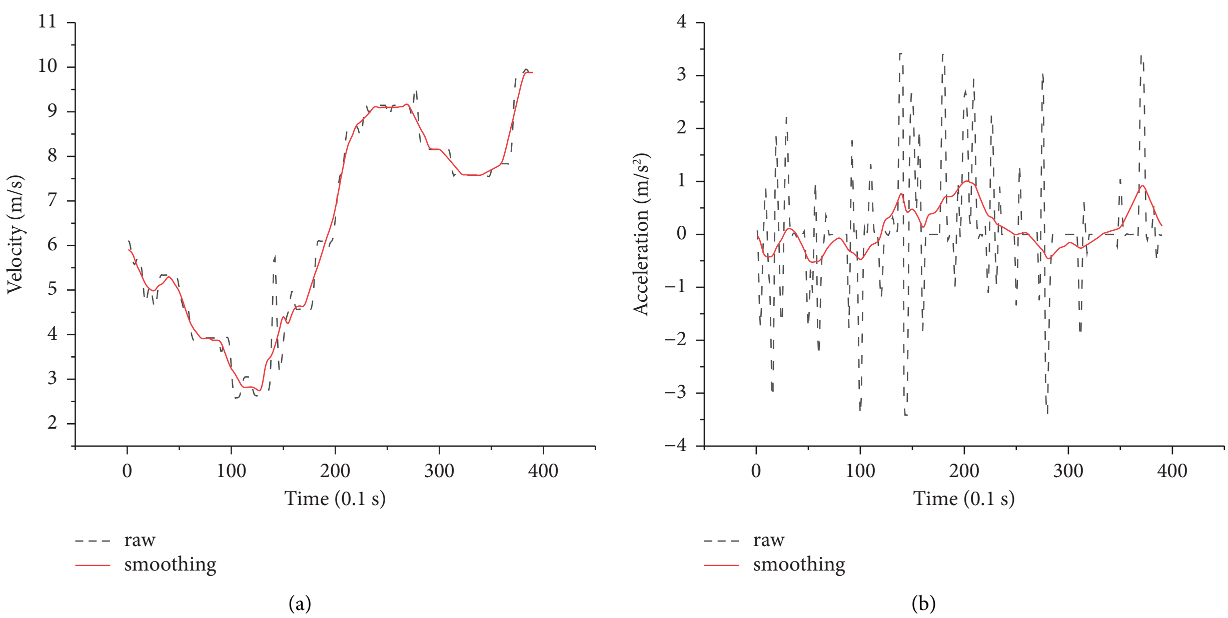

FIGURE 2: Vehicle trajectory reconstruction. (a) Velocity smoothing. (b) Acceleration smoothing.

2.3. Extraction of Driver's Visual Characteristics. Conventional studies on car-following behavior often employ input variables such as following car velocity, relative velocity, and distance to obtain the following car's acceleration. However, psychological research suggests that drivers are unable to accurately perceive speed and distance information. Moreover, their judgments of the distance to the leading vehicles (LVs) are not based on these parameters. Car-following behavior fundamentally constitutes a driver's response to external traffic stimuli. These stimuli primarily originate from the LVs and directly impact the driver's visual perception. As the visual stimuli from the LVs change, drivers adopt various actions (such as maintaining a steady speed, accelerating, decelerating, or changing lanes) to achieve the desired following state. To characterize the visual stimuli perceived by drivers, considering both LVs' information and inter-vehicle distance, we introduce the concept of visual angle along with its rate of change, as depicted in Figure 3. The calculation of these parameters is defined by equations (3) and (4):

$$\theta_n(t) = \frac{w_{n-1}}{\Delta x_n(t) - l_{n-1}}, \tag{3}$$

$$\theta_n'(t) = \frac{d\theta_n(t)}{dt} = \frac{\theta_n(t) - \theta_n(t-1)}{\Delta t}. \tag{4}$$

In equation (3), $\theta_n(t)$ represents the visual angle of the FV's driver at time t, w_{n-1} is the width of the LV, $\Delta x_n(t)$ is the headway between the LV and the FV at time t (space headway), l_{n-1} is the length of the LV, $l_{0,n-1}$ is the distance from the rear of the LV to the front of the FV, and $\theta_n'(t)$ is the change rate of the visual angle of the FV's driver at time t. The sampling interval Δt is 0.1 s.

By combining equations (3) and (4), visual angle and its rate of change sequences can be extracted for each car-following segment. To mitigate the impact of outliers, a two-step threshold cleaning method [29] is employed to cleanse the data. Firstly, the 98th percentile values of both variables are selected as the thresholds for the initial cleansing step, eliminating extreme outliers. The postcleansing data

Table 1: Sample statistics of effective following fragments.

Road	Vehicle number	Effective fragments	Sample number	Duration (min)
I-80	2030	2104	1193900	1989.833
US-101	3879	4031	2364904	3941.507

Table 2: Sample statistics of heterogeneous car-following segments.

Road	Types	S-S	S-L	L-S	L-L
I-80	Number	525	430	487	662
	Duration (s)	887.8	757.6	752.5	1106.5
US-101	Number	1153	755	813	1310
	Duration (s)	1976.2	1371.4	1330.9	2454.9

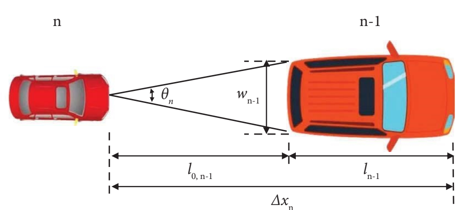

Figure 3: Schematic diagram of driver visual angle calculation.

distribution is depicted in Figures 4(a) and 4(b). Subsequently, guided by the distribution plots, an upper limit of 0.8 is applied to the visual angle (corresponding to 1.25 times the vehicle width based on equation (3)) and a range of ±0.1 rad/s is set as the upper and lower bounds for the visual angle rate of change. The resulting cumulative distribution of cleansed data is shown in Figures 4(c) and 4(d). Following the two-step cleansing process, visual angles are consistently distributed within the range of 0 to 0.8 rad, thereby further eliminating segments associated with congestion. Similarly, the rate of change of visual angle remains within the ±0.1 rad/s range, aligning with the expected visual variation characteristics of drivers under normal driving conditions.

2.4. Numerical Analysis of Visual Characteristics. To gain a deeper understanding of the performance of visual angle and its rate of change variables under different vehicle types, numerical simulations are conducted based on equations (3) and (4). A comparison is made between the visual angle variable and the traditional car-following gap in various vehicle types. Initially, equation (3) is substituted into equation (4) and further manipulated as follows.

$$\begin{aligned}\theta' &= \frac{\theta_1 - \theta_0}{\Delta t}\\ &= \frac{(l_{n-1}/l_1) - (l_{n-1}/l_0)}{\Delta t}\\ &= \frac{l_{n-1}}{\Delta t}\cdot\left(\frac{1}{l_0+\Delta x} - \frac{1}{l_0}\right),\end{aligned} \tag{5}$$

where $\Delta x = l_1 - l_0 = \Delta v \cdot \Delta t$ represents the change in space headway of the FVs at time Δt, Δv represents the relative velocity of vehicles, l_0 represents the current time's space headway, and l_1 represents the next time's space headway. Based on the extracted car-following segment samples, the mean of l_1 is −0.36 m/s, with a minimum of −8.84 m/s and a maximum of 14.77 m/s, and hence it can be taken as $-1.5\,\mathrm{m} \le \Delta x \le 1.5\,\mathrm{m}$.

The numerical simulation of the visual angle variable is depicted in Figure 5. It is evident that as the space headway reduces, the visual angle gradually increases, with a larger increase observed when the headway is small. This suggests that drivers are more significantly influenced by the LVs when the headway is tight. Additionally, for smaller headway, the visual angle increases notably with an increase in vehicle width. However, at greater distances, the differences in visual angle among vehicles with different widths diminish, indicating that at longer distances, the stimuli from vehicles of varying widths remain relatively consistent, and drivers tend toward a state of free driving.

Concerning the visual angle rate of change variable, as indicated by equation (5), it varies with both space headway l_0 and Δx. Figure 6 illustrates the distribution surfaces of the visual angle rate of change concerning Δx under four vehicle width scenarios. Similarly, at longer headway, the visual angle rate of change tends to converge to a single plane and approaches zero for various vehicle widths. However, at smaller headway, significant differences in the visual angle rate of change emerge among different vehicle widths. Larger vehicle widths correspond to larger visual angle rate of changes. In summary, visual angle and its rate of change, as visual characteristic variables of drivers, effectively reflect the diversity in stimuli perception by drivers for different vehicle types at varying distances, aligning more closely with drivers' real-world car-following behaviors.

3. Analysis of Heterogeneous Car-Following Behaviors Based on Visual Characteristics

The numerical simulation results presented earlier find validation in real-world driving situations. When following larger LVs, drivers often adopt more cautious driving behaviors, such as reducing vehicle speed or increasing space headway. This conservative response is attributed to the greater visual stimuli produced by larger vehicles, which also increases the psychological load on drivers. Hence, drivers tend to opt for safer driving strategies. In this section, real driving data will be utilized to compare the disparity between traditional car-following variables and visual characteristic variables across different car-following types. Furthermore, the significance of visual characteristic variables in modeling heterogeneous car-following behaviors will be analyzed.

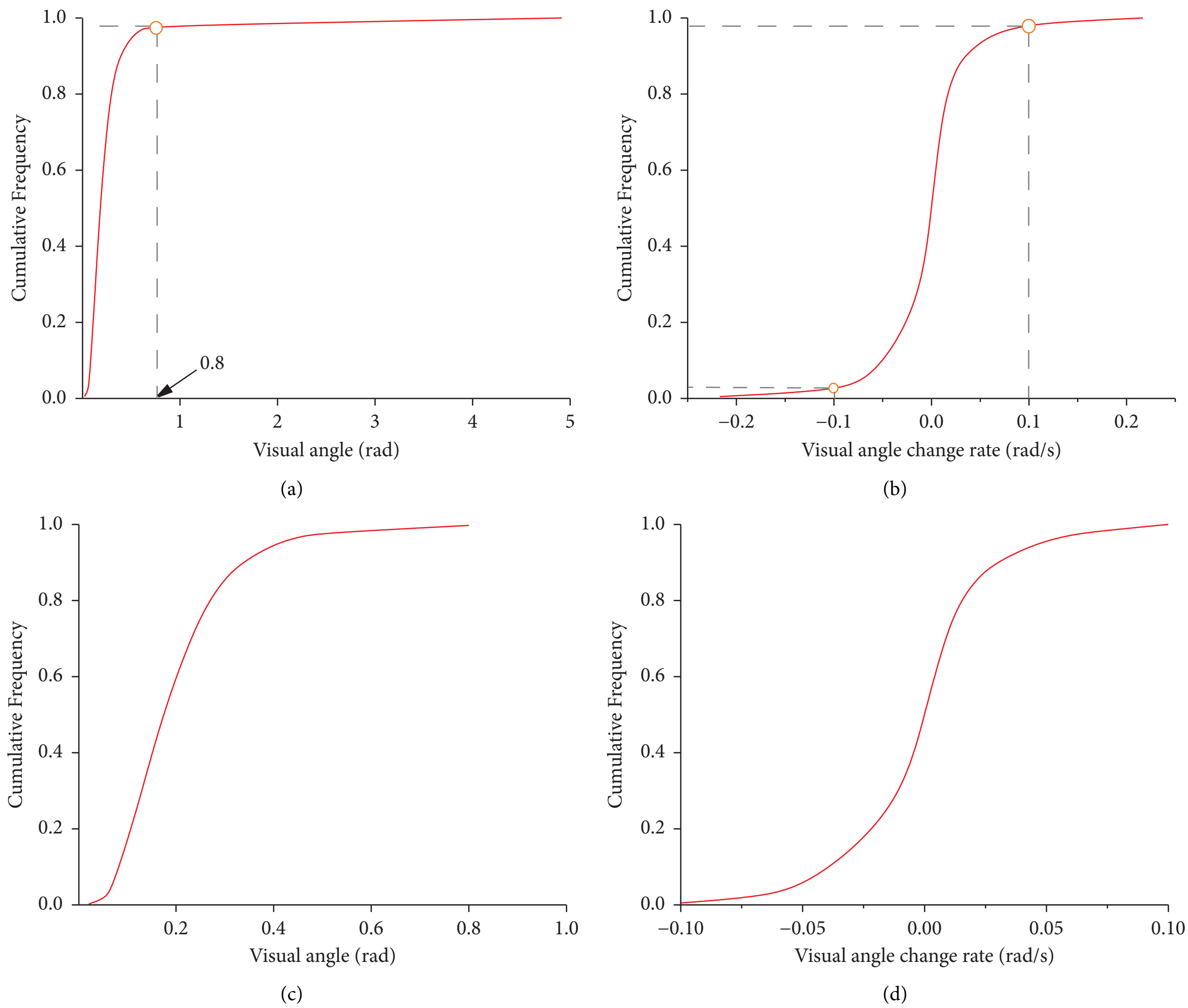

FIGURE 4: Comparison of distribution before and after data cleaning. (a) Visual angle before cleaning. (b) Visual angle change rate before cleaning. (c) Visual angle after cleaning. (d) Visual angle change rate after cleaning.

3.1. Correlation Analysis of Car-Following Variables. Firstly, the min-max normalization technique is employed to mitigate differences stemming from varying scales among different features. Subsequently, partial correlation coefficients are calculated between different features using the method outlined in [30]. The correlation matrices of I-80 and US-101 roads are shown in Figures 7(a) and 7(b), respectively, where the horizontal and vertical axes denote following vehicle (FV) speed and acceleration, visual angle and its change rate, leading vehicle (LV) speed, space headway, and relative speed. According to [31], when the absolute value of a correlation coefficient is between 0 and 0.09, it is considered as having no or very weak correlation. A correlation coefficient between 0.1 and 0.3 is considered weak, 0.3 to 0.5 is considered moderate, and 0.5 to 1.0 is considered a strong correlation. The analysis reveals a substantial correlation between visual angle and space headway, both of which exhibit strong correlation with FV speed (correlation coefficient: ±0.74 of I-80 and ±0.78 of US-101). Similarly, the correlation between visual angle change rate and relative speed is noteworthy, exhibiting similar strong correlation with FV acceleration (correlation coefficients: −0.57, 0.61 of I-80 and −0.59, 0.64 of US-101). Consequently, visual angle and its change rate features can potentially replace traditional space headway and relative speed, rendering the analysis of car-following behavior from the perspective of driver visual characteristics a feasible approach.

3.2. Heterogeneous Car-Following Behavior Analysis. To analyze the disparities in car-following behavior among heterogeneous vehicle combinations, it is necessary to extract stable car-following segments. The extracted segments for analysis have a duration exceeding 30 seconds. Given the dynamic nature of car-following behavior, where drivers continuously adjust their actions in response to real-time stimuli from LVs, the duration of stable car-following segments is significant. For a comprehensive portrayal of micro-level driving behaviors, further small sample

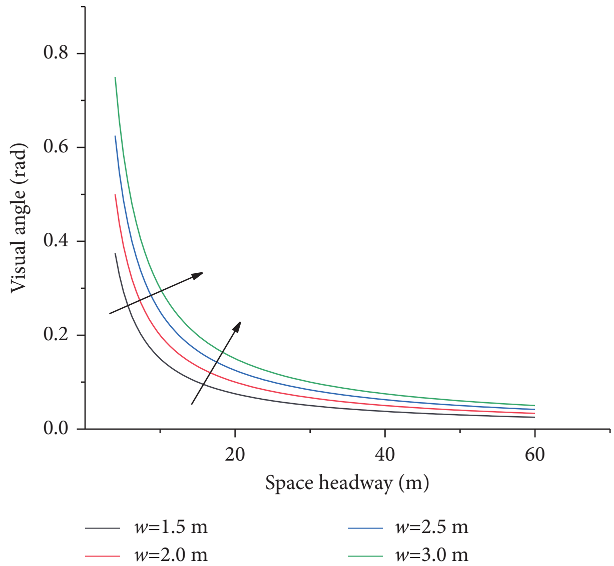

FIGURE 5: Numerical simulation of visual angle under different vehicle widths.

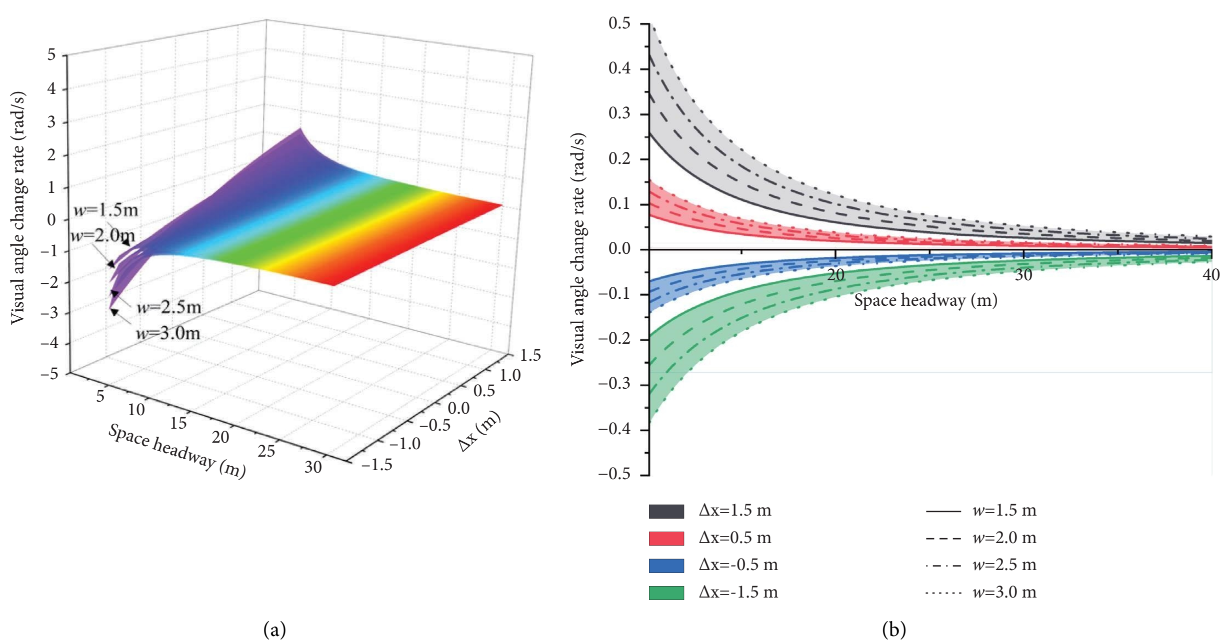

FIGURE 6: Distribution characteristics of visual angle change rate. (a) Numerical simulation of visual angle change rate under different vehicle widths. (b) Evolution characteristics of visual angle change rate under different vehicle widths.

extraction is performed using a time window of 3 seconds and an overlap of 1 second based on the stable car-following segments as depicted in Figure 8. This process yields 35,044 samples for the I-80 road and 71,334 samples for the US-101 road. For each small sample segment, the mean following vehicle speed, mean headway distance (MHD), mean visual angle (MA), mean relative speed, and mean acceleration are extracted as corresponding car-following features. These features serve as the foundation for analyzing heterogeneous car-following behaviors across different vehicle types.

To elucidate the disparities in car-following behavior types across various driving conditions, the average headway distance (MHD) and mean visual angle (MA) for each car-following type are examined within distinct car-following vehicle speed ranges, as indicated in Table 3. The values within parentheses indicate the growth rate of the car-following features when transitioning from a small car leading to a large car [28]. The analysis reveals that with increasing car-following vehicle speed, the headway distance significantly increases while the visual angle decreases

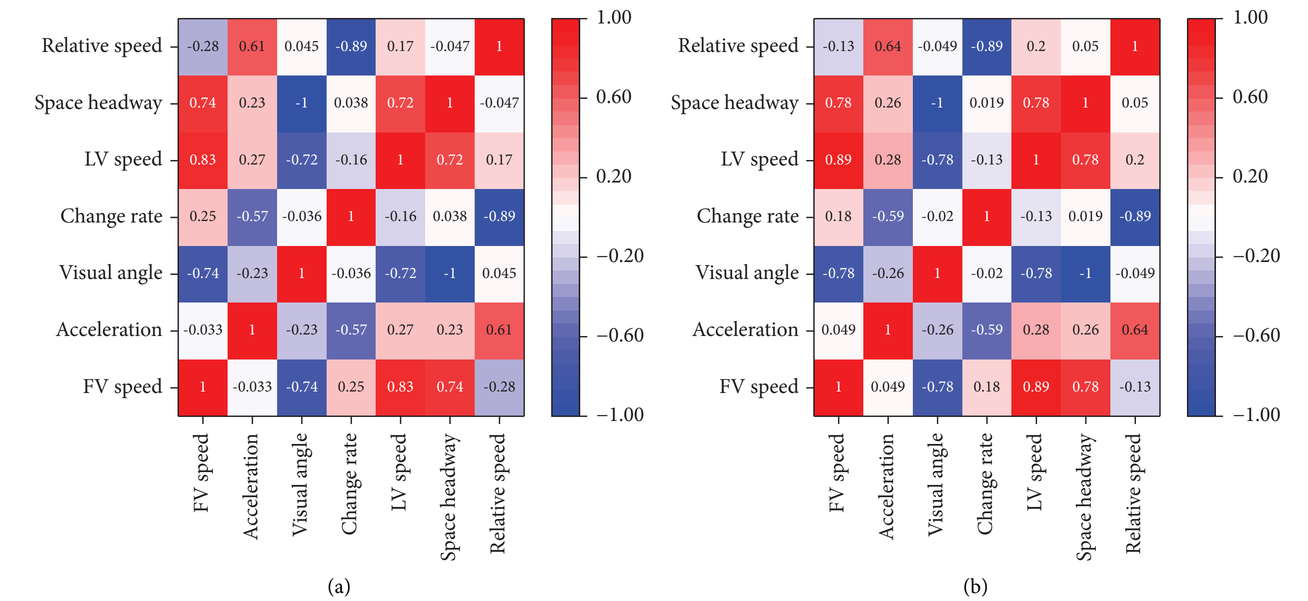

Figure 7: Correlation coefficient matrix of car-following features. (a) Feature matrix of I-80. (b) Feature matrix of US-101.

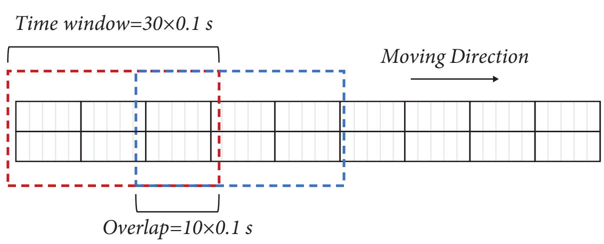

Figure 8: Sketch of small sample fragment extraction.

notably. This suggests that at higher speeds, drivers tend to maintain a safer driving state, resulting in a larger following distance or reduced visual stimulation. Furthermore, across different speeds, the shift from a small car leading to a large car is associated with a respective 7.53% increase (S-S to S-L) and 7.37% increase (L-S to L-L) in average headway distance. In contrast, the visual angle exhibits a more substantial increase of 22.32% (S-S to S-L) and 29.17% (L-S to L-L). This significant increase is attributed to the ability of the visual angle to reflect drivers' sensitivity to the stimulus of the LV size. The visual angle variable effectively captures this sensitivity from both physiological and psychological perspectives, highlighting its crucial role in describing car-following behavior. The same conclusions are drawn from the analysis of the US-101 road.

Subsequently, using car-following type as a categorical variable, one-way ANOVA is conducted on the normalized data to explore the differences in headway distance and visual angle distributions across car-following types. Tables 4 and 5 illustrate that both the mean gap distance (MGD) and mean angle (MA) variables exhibit statistically significant differences across the four car-following types. Subsequent quantification using η^2 (partial eta-squared) and Cohen's f values further affirms this difference. For both the I-80 and US-101 roads, significant differences are identified in MGD and MA among different car-following types. When following larger vehicles, both MGD and MA significantly increase. The quantification analysis reveals that the differences in MGD and MA among various car-following types are 0.5% and 3.6%, respectively. Corresponding Cohen's f values are 0.074 and 0.192, signifying that the visual angle variable effectively captures the differences among different car-following types. This variable reveals the physiological and psychological stress experienced by drivers when facing vehicles of different sizes.

4. Model Calibration and Validation Results

4.1. Constructing Car-Following Models Based on Visual Characteristics. Calibration results from existing highway data models reveal that the FVD (full velocity difference) model outperforms other car-following models such as the GHR model and the Gipps model, demonstrating advantages including higher calibration accuracy, fewer parameters with clear physical significance, and robustness [32]. To comprehensively compare the differential modeling effects of visual characteristic variables and traditional variables in car-following behavior, this study selects the FVD model based on headway distance and the DVA (drivers' visual angle) model based on visual angle for calibration and validation. The FVD model is represented by equations (6) and (7).

$$a_n(t) = \alpha\{V[\Delta x_n(t)] - v_n(t)\} + \lambda \Delta v_n(t), \tag{6}$$

$$V[\Delta x_n(t)] = V_1 + V_2 \tan h[c_1(\Delta x_n(t) - l_{n-1}) - c_2], \tag{7}$$

where $a_n(t)$ denotes the acceleration of the following vehicle at time t, $V[\Delta x_n(t)]$ is the driver's desired speed function based on headway distance, and α, λ, V_1, V_2, c_1, and c_2 are the model parameters.

Table 3: Statistics of average headway and visual angle under different following models on I-80 road.

Road	I-80											
Following types	S-S			S-L			L-S			L-L		
Following velocity (km/h)	Sample size	MHD (m)	MA (rad)	Sample size	MHD (m)	MA (rad)	Sample size	MHD (m)	MA (rad)	Sample size	MHD (m)	MA (rad)
0~10	496	11.25	0.327	377	13.001 (+15.6)***	0.357 (+9.2)***	409	11.423	0.309	473	12.469 (+9.2)***	0.365 (+18.2)***
10~20	2141	14.333	0.226	1740	15.404 (+7.5)***	0.272 (+20.4)***	1750	14.744	0.215	2713	16.184 (+9.8)***	0.266 (+23.7)***
20~30	3826	17.872	0.165	3391	18.696 (+4.6)***	0.208 (+26.1)***	3360	18.408	0.161	5014	19.902 (+8.1)***	0.196 (+21.7)***
30~40	2094	22.169	0.126	1843	22.715 (+2.5)**	0.158 (+25.4)***	1742	22.307	0.127	2579	22.847 (+2.4)***	0.159 (+25.2)***
40~50	296	27.668	0.098	212	25.511 (−7.8)	0.128 (+30.6)***	237	29.311	0.091	276	28.327 (−3.4)	0.118 (+29.7)***
50+	25	38.013	0.068	13	37.005 (−2.7)	0.085 (+25.0)	27	37.31	0.076	10	26.5 (−28.9)*	0.119 (+56.6)**
Average increase					+7.53	+22.32					+7.37	+29.17

Note that the Mann–Whitney *U* test was employed, where ***, **, and * denote significance levels of 1%, 5%, and 10%, respectively. Values within parentheses signify the growth rate of car-following features when transitioning from a small car leading to a large car within the same car-following vehicle type. Cases with significance levels exceeding 5% were disregarded.

Table 4: Results of one-way analysis of variance of following behavior of heterogeneous vehicle on US-101 road.

Variables	Following types	Sample size	Mean	Standard deviation	F	P	Partial η^2	Cohen's f value
Mean gap distance (MGD)	S-S	8878	0.134	0.085	63.49	<0.001***	0.005	0.074
	S-L	7576	0.143	0.085				
	L-S	7525	0.139	0.088				
	L-L	11065	0.151	0.097				
	Overall	35044	0.142	0.09				
Mean angle (MA)	S-S	8878	0.205	0.123	430.554	<0.001***	0.036	0.192
	S-L	7576	0.256	0.138				
	L-S	7525	0.197	0.122				
	L-L	11065	0.249	0.142				
	Overall	35044	0.228	0.135				

Note: ***, **, and * represent significance levels of 1%, 5%, and 10%, respectively.

Table 5: Results of one-way analysis of variance of following behavior of heterogeneous vehicle on I-80 road.

Variables	Following types	Sample size	Mean	Standard deviation	F	P	Partial η^2	Cohen's f value
Mean gap distance (MGD)	S-S	19762	0.086	0.055	16.709	<0.001***	0.001	0.027
	S-L	13714	0.089	0.054				
	L-S	13309	0.09	0.059				
	L-L	24549	0.088	0.058				
	Overall	71334	0.088	0.057				
Mean angle (MA)	S-S	19762	0.165	0.114	972.8	<0.001***	0.039	0.202
	S-L	13714	0.206	0.124				
	L-S	13309	0.163	0.11				
	L-L	24549	0.216	0.133				
	Overall	71334	0.19	0.124				

Note: ***, **, and * represent significance levels of 1%, 5%, and 10%, respectively.

To evaluate the performance of visual angle and its rate of change variables on heterogeneous vehicle types, the visual angle and its rate of change variables extracted are incorporated into the improved FVD model, creating the DVA model. This model has been validated through stability analysis and numerical simulation [33]. The specific form of the model is presented in equations (8) and (9).

$$a_n(t) = \alpha\{V[\theta_n(t)] - v_n(t)\} + \lambda\theta^{'}(t), \tag{8}$$

$$V[\theta_n(t)] = V_1 + V_2 \tan h\left[c_1\left(\frac{w_{n-1}}{\theta_n(t)}\right) - c_2\right], \tag{9}$$

where $V[\theta_n(t)]$ represents the driver's desired speed function based on visual angle.

4.2. Driver Reaction Time Calibration. During car-following processes, individual drivers exhibit variations in their reaction times [34]. In this study, the two-related sequences coefficient method [35] is employed to calibrate driver reaction times at the individual level. Based on prior research, the relative speed and acceleration of the preceding and following vehicles are used for calculation. The specific procedure involves predefining a series of reaction time values at intervals of 0.2 seconds within the range of 0–2 seconds. For each reaction time value, the correlation coefficient between relative speed and acceleration is computed. The reaction time corresponding to the maximum correlation coefficient is selected as the calibrated reaction time for that driver. The distribution of the maximum correlation coefficients for each driver's two sequences is shown in Figure 9(a). The two sequences exhibit a high correlation, with reaction times primarily falling within the range of 1.0–1.6 seconds.

After obtaining the calibrated reaction times for each driver, the distribution of reaction times for different-sized vehicles is compared (Figure 9(b)). The distribution curve for larger vehicles shifts toward the lower right corner, and the percentage of vehicles with reaction times exceeding 1.4 seconds or less than 1.8 seconds is higher for larger vehicles compared to smaller ones. This suggests that the distribution of reaction times for larger vehicles is more dispersed. Statistical analysis conducted on different-sized vehicles from the two roadways reveals that larger vehicles have a 0.458-meter increase in width, representing a 26.4% rise. Furthermore, the average reaction time increases by 0.33 seconds, indicating a 2.8% increment. Specifically, the average reaction time for larger vehicles is 1.212 seconds, while it is 1.178 seconds for smaller vehicles. The standard deviation also increases by 0.434 seconds. This can be attributed to the inherent characteristics of larger vehicles, including their acceleration, deceleration capabilities, and inertia.

4.3. Error Index Selection and Improvement. To assess the disparity between model calibration results and actual outcomes, it is essential to establish appropriate error evaluation metrics and criteria. In past car-following model calibrations, parameters like car-following speed or headway distance have been commonly employed as evaluation

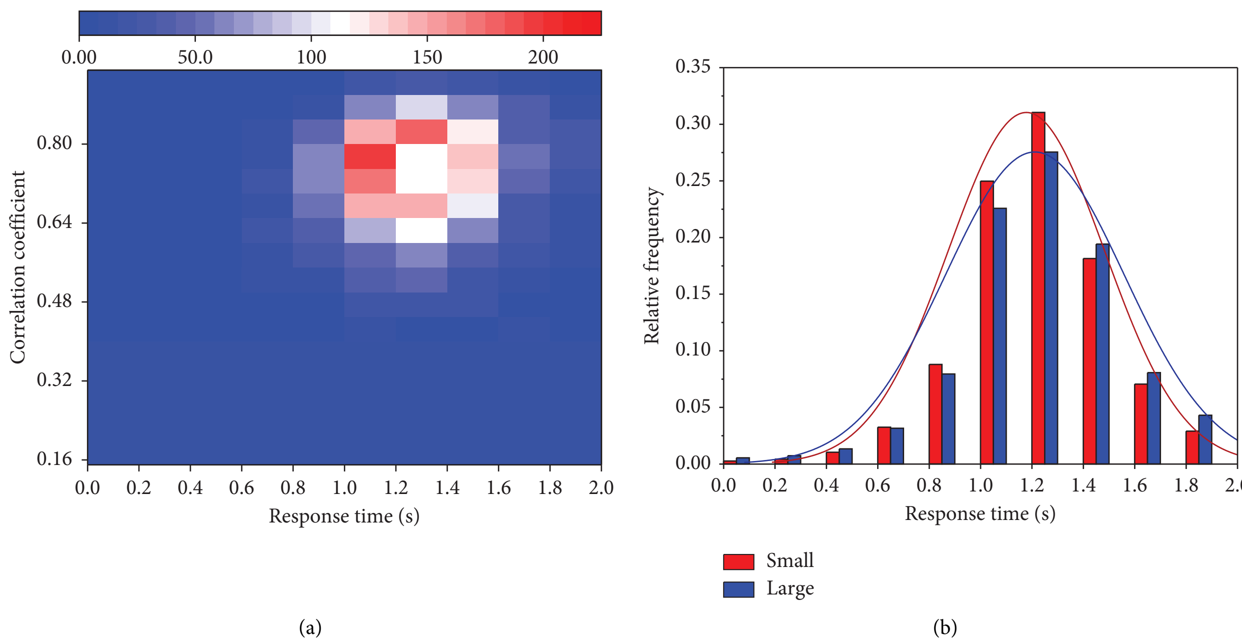

Figure 9: Correlation coefficient and reaction time distribution. (a) Distribution of correlation coefficients. (b) Distribution of response time.

indicators [36–39]. In this study, to contrast the modeling efficacy of headway distance and visual angle, both car-following speed and headway distance variables are adopted as evaluation indicators. Furthermore, the changes in evaluation outcomes under different weightings are analyzed.

As the error indicators, car-following speed and headway distance are chosen. The mean absolute relative error (MARE) is employed as the evaluation function to compare the goodness of fit of the models. The objective function is defined as follows.

$$\mathrm{MARE}(v,\Delta x) = w_1 \times \mathrm{MARE}(v) + w_2 \times \mathrm{MARE}(\Delta x), \quad (10)$$

$$\mathrm{MARE}(y) = \frac{1}{T} \cdot \frac{\sum_{i=1}^{T} \left| y_i^{\mathrm{real}} - y_i^{\mathrm{pre}} \right|}{\sum_{i=1}^{T} y_i^{\mathrm{real}}}, \quad (11)$$

$$w_1 + w_2 = 1, \quad (12)$$

where $\mathrm{MARE}(v,\Delta x)$ represents the comprehensive average percentage error of car-following speed and headway distance and $\mathrm{MARE}(v)$ and $\mathrm{MARE}(\Delta x)$, respectively, denote the average percentage errors of car-following speed and headway distance. T represents the number of data points in the car-following segment. v_i^{real} and $\Delta x_i^{\mathrm{real}}$ represent the actual speed and actual headway distance of the following car at time i, while v_i^{pre} and $\Delta x_i^{\mathrm{pre}}$ denote the model-predicted car-following speed and headway distance at the same time. w_1 and w_2 are the weighting coefficients for the relative speed error and headway distance error, respectively, both initially set to 0.5 during the initial calibration.

4.4. Calibration and Validation of the Overall Samples. Five hundred car-following segments were selected randomly from both I-80 and US-101 highways for calibration and validation using a genetic algorithm combined with a 5-fold cross-validation approach [39]. Among these, 400 segments were designated for calibration, while the remaining 100 segments were reserved for validation. The model parameter calibration outcomes are detailed in Table 6. The results indicate that the DVA model exhibited calibration errors below 0.5 for both roadways. Conversely, the FVD model displayed calibration errors nearing 0.8, marking an increase of 51.93% and 42.22% for the I-80 and US-101 segments, respectively. Furthermore, the standard deviation of the FVD model's calibration results also exhibited significant augmentation.

The parameter means obtained after calibration were employed as model parameters for validation on the reserved dataset. The validation results are presented in Table 7, while the cumulative distribution of calibration and validation errors is depicted in Figure 10. The I-80 road's validation error decreased from 1.409 to 0.611, resulting in a precision improvement of 56.61%. Similarly, the US-101 road's validation error decreased from 1.425 to 0.780, leading to a 45.26% enhancement in precision. The combined improvement across the two roadways was 50.94%. The calibration and validation outcomes across both roadways underscore the superior precision of the DVA model in comparison to the FVD model.

Further investigation into the relationship between error and sample duration is illustrated by the error distribution against the car-following duration, as depicted in Figure 11. The linear fitting of the two models' errors with respect to sample duration shows that both models' errors increase in

Table 6: Overall calibration results of the model.

Road	Sample size	Model		c_1	c_2	v_1 (m/s)	v_2 (m/s)	α	λ	Error
I-80	400	DVA	Mean	6.755	11.528	4.228	3.908	0.079	3.684	0.370
			Std. dev.	6.084	5.674	2.609	2.417	0.091	6.677	0.238
		FVD	Mean	8.578	10.640	4.141	4.262	0.211	0.677	0.769
			Std. dev.	6.330	5.787	2.889	3.107	0.345	4.095	0.929
US-101	400	DVA	Mean	7.258	11.609	6.141	5.957	0.079	4.949	0.453
			Std. dev.	6.223	5.736	3.907	4.104	0.083	6.516	0.388
		FVD	Mean	9.243	11.097	5.333	5.898	0.206	−0.205	0.784
			Std. dev.	6.439	5.853	3.759	4.010	0.333	1.827	0.878

Table 7: Overall validation results of the model.

Road	Model	Validation error			
		Mean	Std. dev.	Min	Max
I-80	DVA	0.611	0.363	0.061	1.381
	FVD	1.409	1.027	0.160	4.116
US-101	DVA	0.780	0.641	0.060	2.822
	FVD	1.425	1.115	0.087	5.854

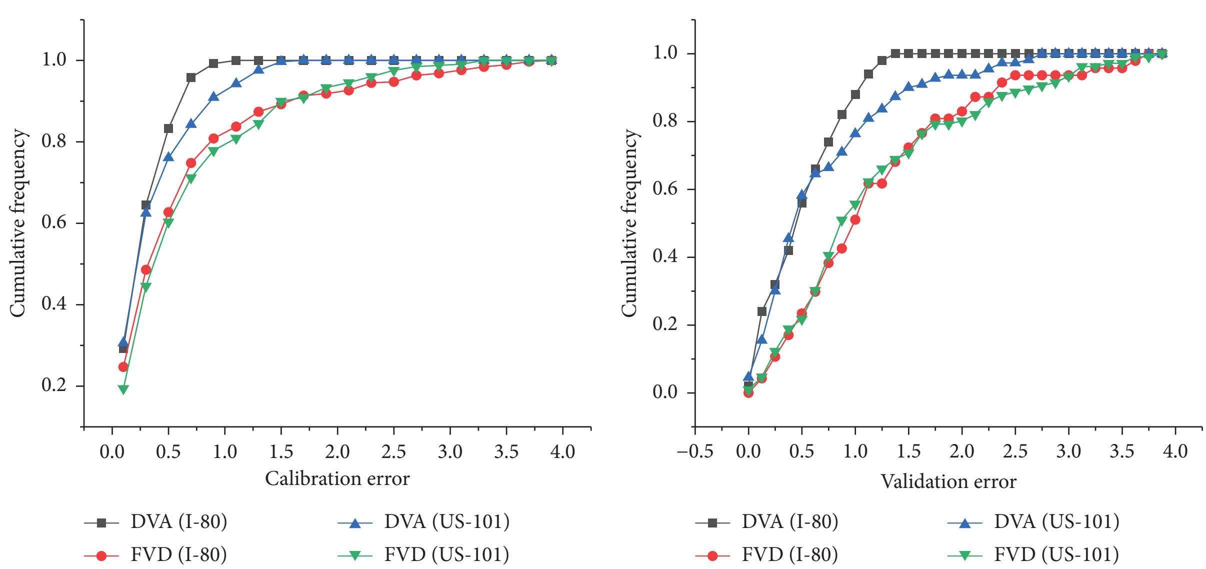

(a) (b)

Figure 10: Cumulative distribution of the overall calibration and validation errors. (a) Cumulative distribution of calibration errors. (b) Cumulative distribution of validation errors.

tandem with sample duration. This indicates that both models are comparably influenced by the sample duration. Additionally, an examination of the FVD model's fitting errors revealed a denser distribution within the 0-1 range, with greater dispersion in fitting errors beyond 1. Consequently, the fitting line shifts upward, indicating higher fitting errors. To elucidate the origin of this discrete error, FVD model calibration results with errors exceeding 1.0 were extracted. Upon categorizing these errors, it was observed that among the two roadways, the L-L type samples accounted for 84 instances, constituting 50.91% of the total. The remaining types were distributed as follows: L-S: 34 instances, 20.61%; S-L: 27 instances, 16.36%; and S-S: 20 instances, 12.12%. This highlights that the increase in FVD model errors primarily stems from the L-L type, signifying that optimal fitting outcomes are achieved when both the lead and following vehicles are small cars. Conversely, as the lead or following vehicle transitions to a large car, the fitting

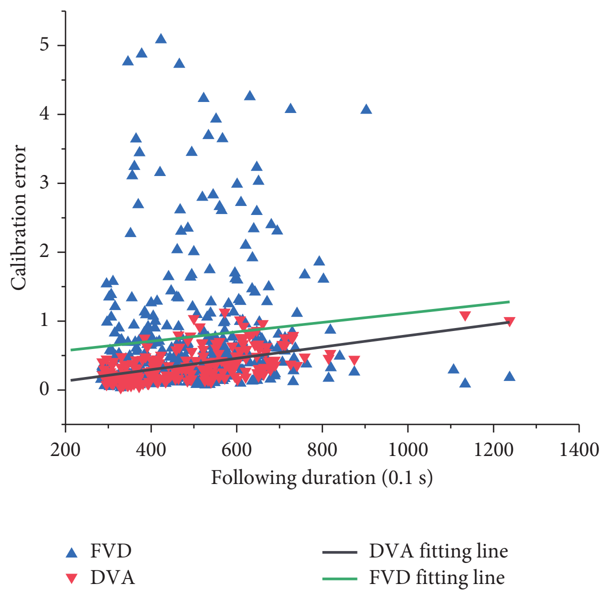

Figure 11: Overall calibration error fitting diagram.

performance diminishes, reaching its poorest state when both are large cars, thus demonstrating a significant degree of error dispersion.

4.5. Calibration and Validation by Different Car-Following Types. To compare the performance of the two models under different car-following scenarios, a subset of car-following samples was selected from various car-following types on the I-80 and US-101 highways. Specifically, 300 samples with a car-following duration ≤60 s were randomly chosen. Among these, 200 samples were designated for calibration, leaving 100 for validation. A 3-fold cross-validation method was employed. The model calibration and validation procedures outlined in Section 4.4 were repeated for each of the four car-following types, yielding parameter calibration results as presented in Table 8.

The analysis of the results indicates notable disparities between the DVA and FVD models in terms of sensitivity coefficients α and λ. In the former, λ is significantly larger, while α is significantly smaller, compared to the latter. Moreover, both are comparatively smaller in the FVD model, signifying lower sensitivity to relative velocity and distance, as well as a reduced capacity for differentiation between the two. The heightened sensitivity of the DVA model to changes in visual angle is attributed to the congested traffic conditions on both roadways. Given the prevalent low speeds of drivers, adhering to the expected velocity is challenging, making the direct stimulus from the LVs a prominent influencer on the car-following behaviors.

Furthermore, a comparison of the calibration errors for different car-following types between the two models is illustrated in Figure 12. Across both roadways, the DVA model exhibited a significant improvement in the mean calibration error in comparison to the FVD model. Additionally, the standard deviation of errors for the DVA model noticeably decreased, indicating a more concentrated error distribution. This reduction in error variability underscores the higher stability of the model calibration process. Furthermore, the DVA model displayed a more uniform error distribution across all four car-following types.

Using the optimal parameter means from the calibration results as model parameters, the validation process was conducted on a set of 100 samples from the validation set. The validation results are presented in Table 9. The outcomes reveal significant accuracy improvements across all four car-following types on the I-80 highway, with the highest increase reaching 62.0% for the L-S type. The remaining types exhibited accuracy enhancements exceeding 50%. On the US-101 highway, accuracy improvements varied considerably among different types. For the S-L and L-L types, the model's accuracy increased by 35.8% and 32.3%, respectively. In contrast, for the S-S and L-S types, the model's accuracy is improved by 46.1% and 44.1%, respectively. This indicates that the fitting accuracy of the DVA model is more significantly enhanced when following a small LV. As illustrated in Figure 13, the DVA model incorporating the visual angle variable demonstrated substantial improvement in fitting effectiveness under various car-following types, showcasing its adaptability and stability across different types of car-following combinations.

4.6. Sensitivity Analysis of the Errors. With the multitude of existing car-following models, a unified evaluation standard for model performance remains lacking. To investigate the performance of both models under different evaluation criteria, by assigning different weights to the space headway and speed, we improve the traditional error functions seeing in equations (11) and (12). A series of values are set for w_1 and w_2, and 400 samples are randomly selected from I-80 road and US-101 road for calibration. The calibration results are illustrated in Figure 14. It is evident from these results that when w_1 is equal to 0 (at this moment, w_2 equals 1), considering only the headway as the error indicator, both model errors for all four scenarios reach their maximum. As w_1 increases, the errors for both models gradually decrease. When w_1 equals 1 (w_2 equals 0), with consideration solely given to the following vehicle's speed, the error reaches its minimum.

Further comparison reveals that the FVD model exhibits substantial discrepancies in fitting results between the two road types, while the DVA model's performance remains similar across both road types. This suggests that the DVA model displays higher adaptability under varying road conditions. As w_1 increases, the error of DVA model decreases slowly, indicating its overall stability, while the FVD model demonstrates a more pronounced decline. This signifies that the DVA model boasts greater robustness against different error indicators, resulting in a more consistent model performance. To delve into this phenomenon, a comparison of errors for different indicator weights and combinations is conducted, as illustrated in Figure 15. This analysis reveals that under varying weights, the FVD model shows significant differences in error outcomes among

Table 8: Calibration results of heterogeneous car-following model.

Road	Model	Following types	c_1	c_2	v_1	v_2	α	λ	Calibration error	
									Mean	Std. dev.
I-80	DVA	S-S	6.160	11.877	4.046	4.235	0.076	4.042	0.430	0.292
		S-L	6.482	11.697	4.034	4.180	0.086	4.209	0.399	0.251
		L-S	7.263	11.918	3.546	4.381	0.091	3.952	0.387	0.227
		L-L	7.141	11.465	3.791	4.245	0.080	3.938	0.348	0.223
	FVD	S-S	8.049	11.205	4.052	4.247	0.216	−0.149	0.894	0.941
		S-L	8.711	9.765	4.026	3.956	0.260	−0.106	0.769	0.618
		L-S	9.057	10.472	3.883	4.279	0.275	0.110	0.890	0.976
		L-L	9.569	10.364	4.014	4.171	0.211	−0.213	0.730	0.754
US-101	DVA	S-S	6.385	11.624	5.304	5.592	0.069	6.007	0.455	0.372
		S-L	7.331	11.393	5.819	6.737	0.060	4.927	0.434	0.309
		L-S	7.594	11.580	5.400	6.721	0.063	5.353	0.459	0.389
		L-L	6.570	11.385	5.721	6.573	0.070	4.992	0.424	0.341
	FVD	S-S	8.489	10.950	4.832	4.917	0.176	−0.337	0.905	0.703
		S-L	9.005	10.094	4.955	5.881	0.150	−0.264	0.634	0.612
		L-S	8.227	10.197	5.294	5.121	0.185	−0.332	0.658	0.508
		L-L	7.765	10.545	4.463	6.064	0.181	−0.213	0.727	0.653

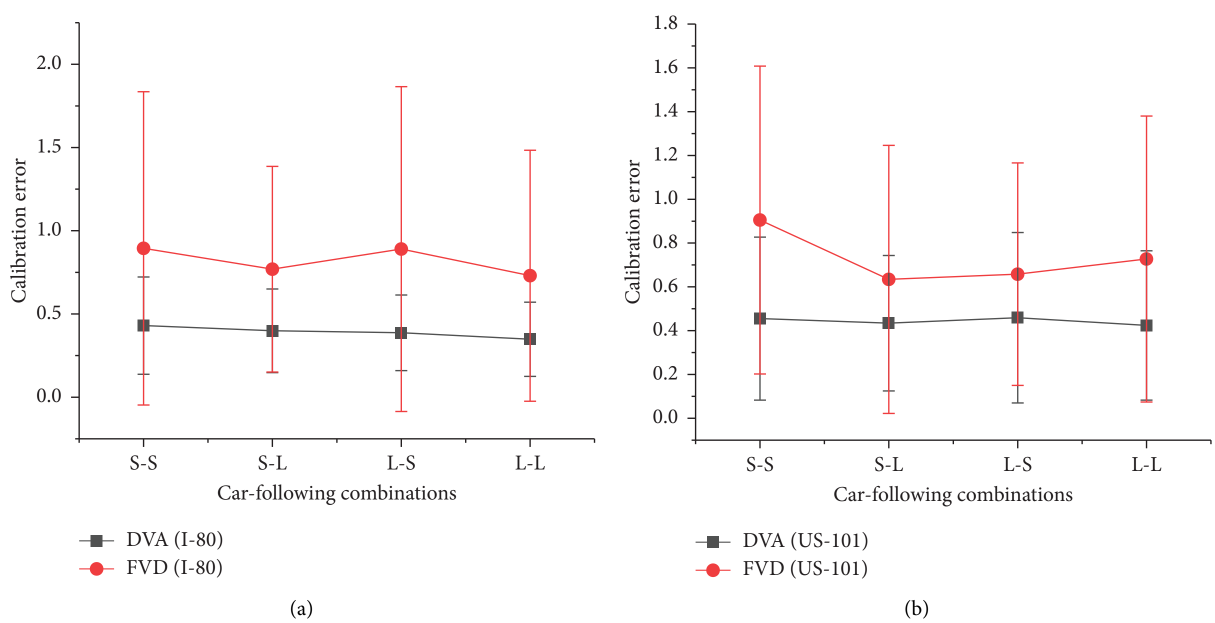

Figure 12: Calibration results of different car-following combinations. (a) Distribution of calibration error at I-80. (b) Distribution of calibration error at US-101.

Table 9: Verification results of heterogeneous vehicle-following model.

Road	Model	S-S	S-L	L-S	L-L
I-80	DVA	0.821	0.835	0.649	0.640
	FVD	1.695	1.886	1.707	1.441
	Accuracy increase (%)	0.515	0.558	0.620	0.556
US-101	DVA	0.663	0.866	0.769	1.013
	FVD	1.231	1.348	1.374	1.496
	Accuracy increase (%)	0.461	0.358	0.441	0.323

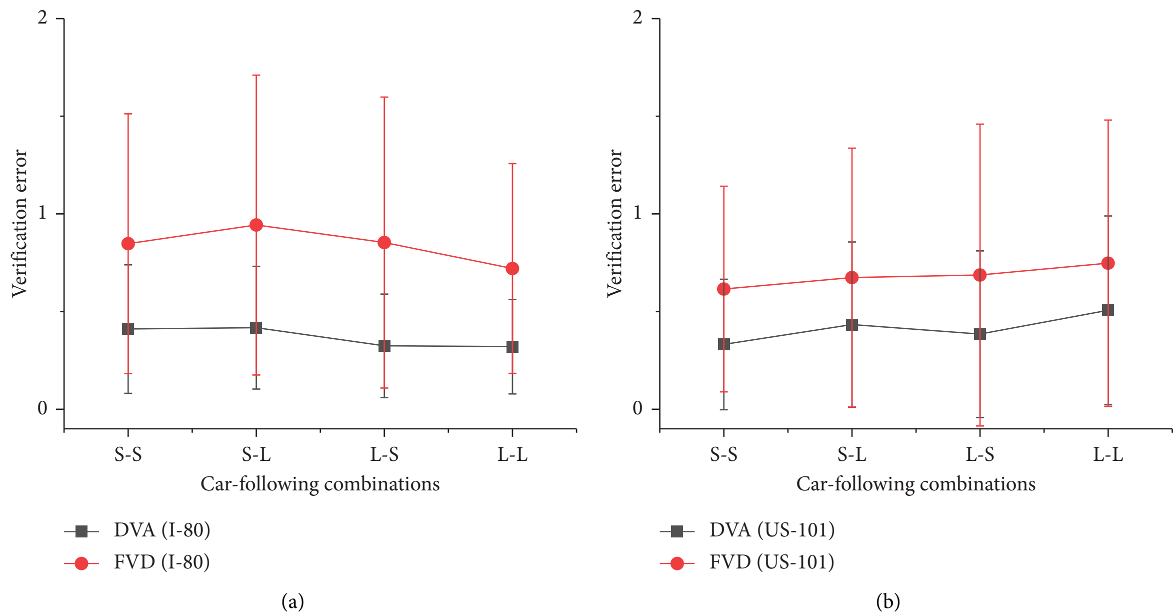

FIGURE 13: Verification results of different car-following combinations. (a) Distribution of verification error at I-80. (b) Distribution of verification error at US-101.

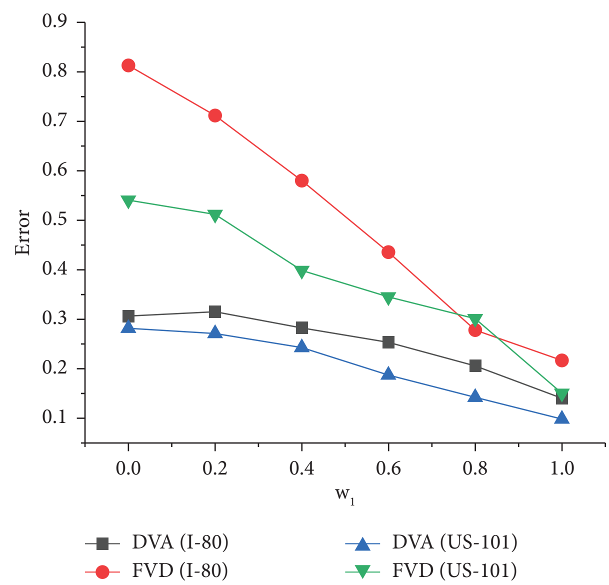

FIGURE 14: Error sensitivity distribution.

different types. Notably, when the current vehicle is a larger vehicle, the model error notably increases. Conversely, the DVA model exhibits smaller variations in error under different types. Combining these findings with the statistical analysis from Section 2.3, we could draw the conclusion that incorporating driver visual angle variables can enhance the model's fitting stability across various vehicle combinations, leading to a better performance.

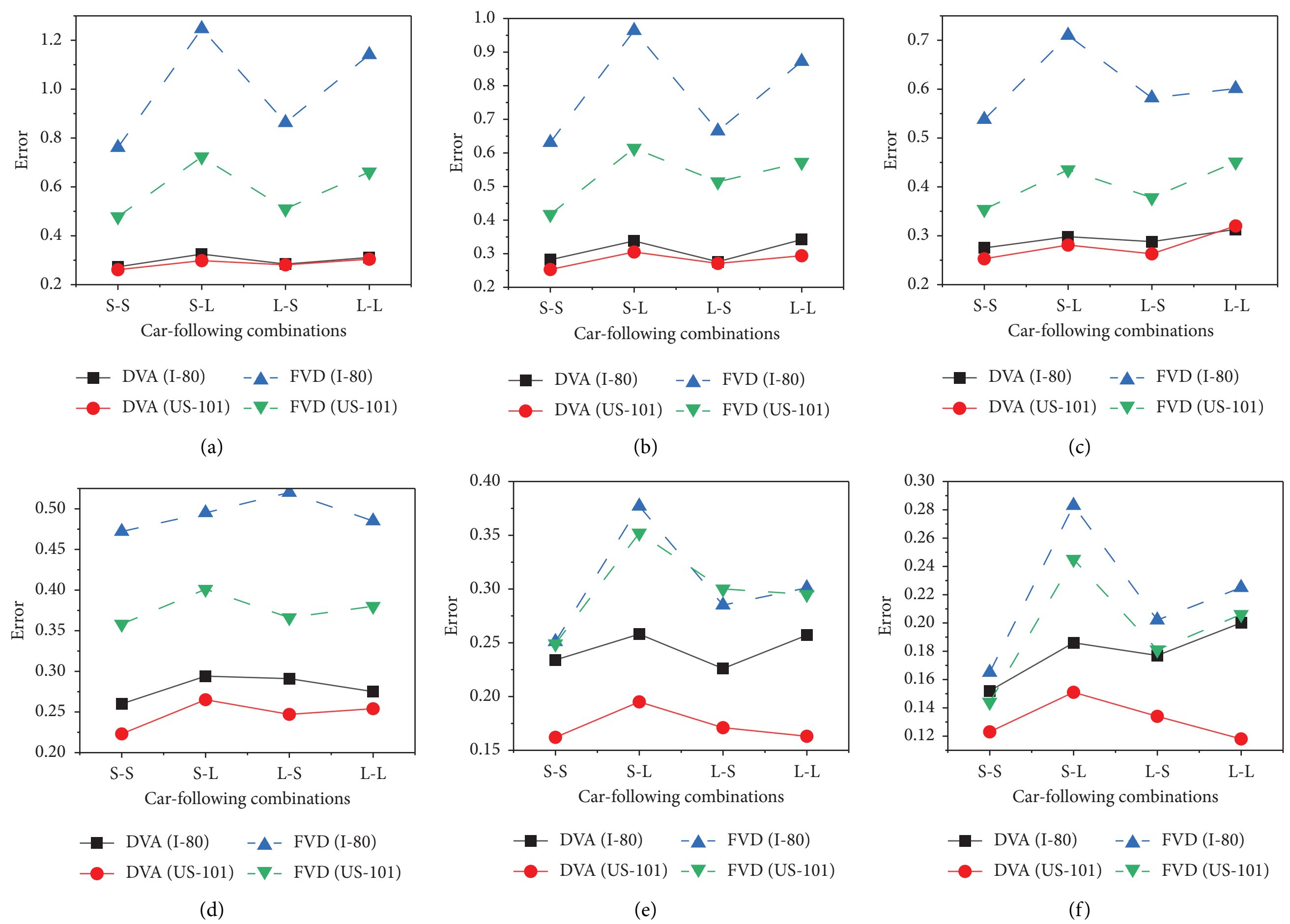

FIGURE 15: Error sensitivity distribution of different car-following combinations. (a) $w_1 = 0.0$, $w_2 = 1.0$. (b) $w_1 = 0.2$, $w_2 = 0.8$. (c) $w_1 = 0.4$, $w_2 = 0.6$. (d) $w_1 = 0.6$, $w_2 = 0.4$. (e) $w_1 = 0.8$, $w_2 = 0.2$. (f) $w_1 = 1.0$, $w_2 = 0.0$.

5. Conclusions

This study is based on heterogeneous car-following segments extracted from the NGSIM dataset. Visual characteristic variables are extracted for numerical simulations and compared with traditional car-following variables to investigate the differences in heterogeneous car-following behaviors. Statistical analysis reveals substantial variability in driver behavior within heterogeneous car-following scenarios. Furthermore, the use of visual characteristic variables effectively reflects the visual stimuli experienced by drivers when following larger vehicles. In contrast to traditional car-following distance variables, these visual stimuli exhibit more pronounced differences across different car-following types, emphasizing the significance of incorporating driver visual characteristics in the study of heterogeneous car-following behaviors.

To evaluate the merits of modeling driver visual characteristics in comparison with traditional car-following variables, both an improved DVA model and an FVD model were calibrated and validated. The results demonstrate that the enhanced DVA model significantly outperforms the FVD model.

The calibration results for different car types and the sensitivity analysis of errors reveal that the DVA model, based on driver visual characteristics, exhibits high adaptability and stability across diverse road conditions, vehicle types, and various error metric weights. This indicates the model's potential for broader application and implementation. Therefore, investigating micro-driving behaviors from the driver's perspective, analyzing physiological and psychological characteristics during driving, refining car-following modeling theories, and addressing the challenges of heterogeneous car-following are of paramount importance.

It should be noted that this study solely focuses on improving the input variables of the FVD model, which yielded significant improvements. However, the potential influence of model structure on different variables cannot be ruled out. Further experimentation is needed for other commonly used models such as the Gipps model and the Wiedemann model. Additionally, the NGSIM dataset features high traffic flow on both roadways, typically involving car-following distances below 50 meters. Drivers are subjected to substantial visual stimuli in such scenarios. As car-following distances increase further, driver stimuli tend to diminish. Analyzing the changing characteristics of driver visual stimuli under relatively smoother traffic flow conditions presents a crucial challenge in understanding driver driving mechanisms.

Data Availability

The NGSIM dataset provided by the Federal Highway Administration (FHWA) was used in this study, and data will be available upon request.

Conflicts of Interest

The authors declare that there are no conflicts of interest.

Acknowledgments

This study was supported by the "Pioneer" and "Leading Goose" R&D Program of Zhejiang (2022C01042), the National Natural Science Foundation of China (grant no. 72361137006), and the Natural Science Foundation of Zhejiang Province (grant no. LR23E080002).

References

[1] L. A. Pipes, "An operational analysis of traffic dynamics," *Journal of Applied Physics*, vol. 24, no. 3, pp. 274–281, 2004.

[2] W. Dian-hai and J. I. N. Sheng, "Review and outlook of modeling of car following behavior," *China Journal of Highway and Transport*, vol. 25, no. 1, p. 115, 2012.

[3] Y. Li, L. Zhang, H. Zheng et al., "Nonlane-discipline-basedcar-following model for electric vehicles in transportation- cyber-physical systems," *IEEE Transactions on Intelligent Transportation Systems*, vol. 19, no. 1, pp. 38–47, 2018.

[4] X. Huang, J. Sun, J. Sun, and J. Sun, "A car-following model considering asymmetric driving behavior based on long short-term memory neural networks," *Transportation Research Part C: Emerging Technologies*, vol. 95, pp. 346–362, 2018.

[5] M. Park, Y. Kim, H. Yeo, and H. Yeo, "Development of an asymmetric car-following model and simulation validation," *IEEE Transactions on Intelligent Transportation Systems*, vol. 21, no. 8, pp. 3513–3524, 2020.

[6] X. Zhang, M. Zhao, Y. Zhang et al., "An improved car-following model based on multiple preceding vehicles under connected vehicles environment," *International Journal of Modern Physics C*, vol. 33, 2022.

[7] W. Yao, J. Yu, Y. Yang et al., "Understanding travel behavior adjustment under COVID-19," *Communications in Transportation Research*, vol. 2, Article ID 100068, 2022.

[8] X. Qu, S. Wang, D. Niemeier, and N. Deb, "On the urban-rural bus transit system with passenger-freight mixed flow," *Communications in Transportation Research*, vol. 2, Article ID 100054, 2022.

[9] T. Tang, J. Zhang, K. Z. Liu, and K. Liu, "A speed guidance model accounting for the driver's bounded rationality at a signalized intersection," *Physica A: Statistical Mechanics and its Applications*, vol. 473, pp. 45–52, 2017.

[10] S. Jin, J. A. Alagbe, D. A. Ma, and D. Ma, "Drivers' phone use behavior at red traffic signals," *IEEE Intelligent Transportation Systems Magazine*, vol. 13, no. 1, pp. 169–180, 2021.

[11] P. Liao, T. Q. Tang, T. Wang, J. Zhang, T. Wang, and J. Zhang, "A car-following model accounting for the driving habits," *Physica A: Statistical Mechanics and its Applications*, vol. 525, pp. 108–118, 2019.

[12] Y. Luo, Y. Chen, K. Lu et al., "On the driver's stochastic nature in car-following behavior: modeling and stabilizing based on the V2I environment," *Electronic Research Archive*, vol. 31, no. 1, pp. 342–366, 2023.

[13] S. C. Calvert and B. Van Arem, "A generic multi-level framework for microscopic traffic simulation with automated vehicles in mixed traffic," *Transportation Research Part C: Emerging Technologies*, vol. 110, pp. 291–311, 2020.

[14] A. Srivastava, D. Chen, S. C. Ahn, and S. Ahn, "Modeling and control using connected and automated vehicles with chained asymmetric driver behavior under stop-and-go oscillations," *Transportation Research Record*, vol. 2675, no. 1, pp. 342–355, 2021.

[15] Y. Huang, R. Jiang, H. Zhang et al., "Experimental study and modeling of car-following behavior under high speed situation," *Transportation Research Part C: Emerging Technologies*, vol. 97, pp. 194–215, 2018.

[16] S. Ossen and S. P. Hoogendoorn, "Heterogeneity in car-following behavior: theory and empirics," *Transportation Research Part C: Emerging Technologies*, vol. 19, no. 2, pp. 182–195, 2011.

[17] S. An, L. Xu, G. Chen, Z. Shi, G. Chen, and Z. Shi, "A new car-following model on complex road considering driver's characteristics," *Modern Physics Letters B*, vol. 34, no. 16, Article ID 2050182, 2020.

[18] Q. Cheng, X. Jiang, W. Wang et al., "Analyses on the heterogeneity of car-following behaviour: evidence from a cross-cultural driving simulator study," *IET Intelligent Transport Systems*, vol. 14, no. 8, pp. 834–841, 2020.

[19] Y. Pan and X. Guan, "Stochastic optimal velocity car-following model based on quantile regression," *Journal of Zhejiang University*, vol. 56, no. 8, pp. 1553–1559, 2022.

[20] M. A. Makridis, A. Anesiadou, K. Mattas et al., "Characterising driver heterogeneity within stochastic traffic simulation," *Transportation Business: Transport Dynamics*, vol. 11, no. 1, pp. 725–743, 2023.

[21] S. Peeta, P. Zhang, W. Zhou, Zhang, and W. Zhou, "Behavior-based analysis of freeway car–truck interactions and related mitigation strategies," *Transportation Research Part B: Methodological*, vol. 39, no. 5, pp. 417–451, 2005.

[22] L. Liu, L. Zhu, D. Z. Yang, and D. Yang, "Modeling and simulation of the car-truck heterogeneous traffic flow based on a nonlinear car-following model," *Applied Mathematics and Computation*, vol. 273, pp. 706–717, 2016.

[23] N. Raju, S. Arkatkar, G. A. Joshi, and G. Joshi, "Modeling following behavior of vehicles using trajectory data under mixed traffic conditions: an Indian viewpoint," *Transportation Letters*, vol. 13, no. 9, pp. 649–663, 2021.

[24] L. Li, R. Jiang, Z. He et al., "Trajectory data-based traffic flow studies: a revisit," *Transportation Research Part C: Emerging Technologies*, vol. 114, pp. 225–240, 2020.

[25] C. Thiemann, M. Treiber, A. Kesting, and K. Arne, "Estimating acceleration and lane-changing dynamics from next generation simulation trajectory data," *Transportation Research Record*, vol. 2088, no. 1, pp. 90–101, 2008.

[26] F. Marczak, C. Buisson, and C. Buisson, "New filtering method for trajectory measurement errors and its comparison with existing methods," *Transportation Research Record*, vol. 2315, no. 1, pp. 35–46, 2012.

[27] C. Chen, L. Li, J. Hu, C. Geng, J. Hu, and C. Geng, "Calibration of MITSIM and IDM car-following model based on NGSIM trajectory datasets," in *Proceedings of the 2010 IEEE*

International Conference on Vehicular Electronics and Safety, pp. 48–53, QingDao, China, July 2010.

[28] Y. Zhang, C. Shao, H. Li, and X. Ma, "Microscopic characteristics of lane-change maneuvers based on NGSIM," *Journal of Transportation Information and Safety*, vol. 33, no. 6, pp. 19–24, 2015.

[29] B. Higgs and M. Abbas, "A two-step segmentation algorithm for behavioral clustering of naturalistic driving styles," in *Proceedings of the 16th International IEEE Conference on Intelligent Transportation Systems (ITSC 2013)*, pp. 857–862, The Hague, Netherlands, October 2013.

[30] L. Zheng, P. J. Jin, H. Huang et al., "A vehicle type-dependent visual imaging model for analysing the heterogeneous car-following dynamics," *Transportation Business: Transport Dynamics*, vol. 4, no. 1, pp. 68–85, 2016.

[31] J. Cohen, *Statistical Power Analysis for the Behavioral Sciences*, Routledge, New York, NY, USA, 1988.

[32] M. Zhu, X. Wang, A. Tarko, S. Fang, A. Tarko, and S. Fang, "Modeling car-following behavior on urban expressways in Shanghai: A naturalistic driving study," *Transportation Research Part C: Emerging Technologies*, vol. 93, pp. 425–445, 2018.

[33] S. Jin, D. H. Wang, Z. Y. Huang, P. F. H. Tao, Z.-Y. Huang, and P.-F. Tao, "Visual angle model for car-following theory," *Physica A: Statistical Mechanics and its Applications*, vol. 390, no. 11, pp. 1931–1940, 2011.

[34] U. Durrani, C. Lee, D. L. Shah, and D. Shah, "Predicting driver reaction time and deceleration: comparison of perception-reaction thresholds and evidence accumulation framework," *Accident Analysis & Prevention*, vol. 149, Article ID 105889, 2021.

[35] X. Ma, I. Andréasson, and I. Andréasson, "Estimation of driver reaction time from car-following data: application in evaluation of general motor–type model," *Transportation Research Record: Journal of the Transportation Research Board*, vol. 1965, no. 1, pp. 130–141, 2006.

[36] B. Kim, M. K. Chang, J. Kim, S. H. Lee, C. Chung, and J. W. Choi, "Probabilistic vehicle trajectory prediction over occupancy grid map via recurrent neural network," in *Proceedinngs of the 2017 IEEE 20th International Conference on Intelligent Transportation Systems (ITSC)*, Yokohama, Japan, October 2017.

[37] L. Yang, S. Zhao, and H. Xu, "Car-following model based on the modified optimal velocity function," *Journal of Transportation Systems Engineering and Information Technology*, vol. 17, no. 2, pp. 41–46+67, 2017.

[38] Z. Sun, X. J. Ban, and X. Jeff Ban, "Vehicle trajectory reconstruction for signalized intersections using mobile traffic sensors," *Transportation Research Part C: Emerging Technologies*, vol. 36, pp. 268–283, 2013.

[39] X. Wang and M. Zhu, "Calibration and verification of a car-following model for Chinese drivers on urban expressways based on natural driving data," *Chinese Journal of Highway and Transport*, vol. 31, no. 9, p. 129, 2018.

[40] V. Punzo, M. Montanino, and M. Montanino, "Speed or spacing? Cumulative variables, and convolution of model errors and time in traffic flow models validation and calibration," *Transportation Research Part B: Methodological*, vol. 91, pp. 21–33, 2016.

[41] W. Xue-song and Z. H. U. Mei-xin, "Calibrating and validating car-following models on urban expressways for Chinese drivers using naturalistic driving data," *China Journal of Highway and Transport*, vol. 31, no. 9, p. 129, 2018.